Hindawi Publishing Corporation
Journal of Sensors
Volume 2016, Article ID 9565208, 7 pages
http://dx.doi.org/10.1155/2016/9565208

Research Article

LG-Mod: A Modified Local Gradient (LG) Method to Retrieve SAR Sea Surface Wind Directions in Marine Coastal Areas

Fabio M. Rana,[1] Maria Adamo,[1] Guido Pasquariello,[1] Giacomo De Carolis,[2] and Sandra Morelli[3]

[1]*Institute of Intelligent Systems for Automation (ISSIA), National Research Council of Italy (CNR), Via Amendola 122/O, 70126 Bari, Italy*
[2]*Institute for the Electromagnetic Sensing of the Environment (IREA), National Research Council of Italy (CNR), Via Bassini 15, 20133 Milan, Italy*
[3]*Department of Physics, Computer Science, and Mathematics, University of Modena and Reggio Emilia, Via Campi 213/a, 41125 Modena, Italy*

Correspondence should be addressed to Fabio M. Rana; rana@ba.issia.cnr.it

Received 29 May 2015; Revised 25 September 2015; Accepted 28 September 2015

Academic Editor: Jose C. Nieto-Borge

This paper describes a novel SAR wind direction estimation method based on the computation of local gradients over quasi-linear and quasi-periodic structures detected by SAR imagery. The method relies upon the standard LG method for the part relevant to the computation of the local gradients. The novelty is that the dominant local wind direction and related accuracy are estimated using results derived from the Directional Statistics. The LG-Mod is validated against in situ coastal wind measurements provided by instrumented buoys with 63 ENVISAT ASAR images. Results show an overall agreement with RMSE values obtained for off-shore areas, but residual effects due to the complex phenomena occurring in the proximity of shoreline may degrade the performance when running in automated mode.

1. Introduction

Sea surface wind is a crucial parameter for studies of the several oceanographic applications such as marine meteorology [1, 2], marine oil spill monitoring [3, 4], and wind energy resources [5, 6] among others.

While mesoscale numerical weather models (NWMs) provide reliable wind fields for off-shore areas, in general their accuracy is drastically reduced in the proximity of the shoreline. This is due to the complex land/sea interactions which take place in coastal areas, whose phenomenology is generally poorly described within NWM schemes. In order to overcome such difficulty, accurate observations on regular spatial scale of sea surface winds should feed NWM in order to provide them with useful initial conditions and verification data for reliable coastal wind predictions.

Spaceborne microwave remote sensing of the sea surface has been proved to be effective in monitoring off-shore sea surface phenomena and has reached technological maturity to provide quantitative coastal areas observations.

Surface winds from scatterometer observations are available and can improve NWM forecasts only off-shore.

While spaceborne scatterometry can provide wind vector measurements on global scale, the coarse spatial resolution (10–25 km) hampers application in coastal regions as a result of the obvious land contaminations.

Besides, synthetic aperture radar (SAR) sensors have demonstrated over the past decade their ability to provide accurate wind speed and direction measurements in the ocean. In contrast to scatterometer, the high spatial resolution of SAR imaging (1–10 m) has the potential to capture the typical complex wind fields which characterize coastal regions. Nevertheless, SAR wind field retrieval in marine coastal areas still remains an open issue.

It has been shown in [7] that SAR wind field retrievals which exploit guess wind information coming from NWMs

[8] show strong dependence on the goodness of the input wind vector used as guess. The information coming from SAR is in general unable to fully correct the input NWM wind direction. For this reason, it would be highly desirable to develop methods which provide wind direction independent of external information.

SAR imaging can detect atmospheric and oceanic phenomena which are able to modulate sea surface and hence the backscattered signal, such as boundary layer rolls (BLRs) and wind streaks (WSs).

BLRs are atmospheric roll vortices generated by thermal instabilities which develop within the marine atmospheric boundary layer [9–11]. They can persist over hours or days and are typically associated with unstable or neutral boundary layer conditions [12, 13]. The fluctuations of wind stress at the convergence and divergence zones between rolls [14, 15] make BLRs appear on SAR images as quasi-periodic linear modulation of backscattering with typical spatial scale ranging from 1 to 4 km. As the orientation of BLR axes is in general between the direction of the mean sea surface wind and that of the associated geostrophic wind [14], such directional signature is being widely used to estimate sea surface wind direction from SAR imaging.

WSs are characterized by a narrower spatial modulation (0.1–0.5 km), as showed for the first time in X-band nautical radar images [16]. These features are more closely aligned with the sea surface wind direction and evolve with a lifetime of several tens of minutes. For this reason, wind streaks have been exploited for wind direction retrieval from SAR images [17, 18].

Although BLRs and WSs can provide wind directions, it is an open issue what are the favourable conditions for their visibility on SAR images and, above all, if their rate of occurrence is enough for operational use. Indeed, as stated in [14], the visibility of BLRs on SAR images depends on several factors, such as the SAR operated frequency and polarization, incidence angle, wind speed regime, and wind direction with respect to SAR look geometry. Moreover, in [19] analysis on a large dataset of SAR images assessed that BLR visibility is subjected to an annual seasonality and that cold air flow conditions foster the formation of atmospheric rolls. However, cooccurrence of such factors does not guarantee the presence of related SAR signatures. In contrast, statistics of occurrence of WSs wait to be compiled and factors influencing their occurrence have to be investigated.

Research on SAR wind fields retrieval has focused on the development of methods which aim at extracting the main orientations of wind-induced features from SAR images. Commonly these algorithms identify the main wind directions with 180° ambiguity, which can be resolved by identifying areas of wind shadowing within the SAR image or by using ancillary wind direction information from NWM predictions or in situ data.

A number of SAR-based wind retrieval algorithms have exploited Fourier analysis [20–23] to provide wind direction from BLRs features with spatial resolution up to 10 km and accuracy ranging approximately from 10° to 40° [23, 24]. Working in the spatial domain, two families of algorithms have been developed, both providing high resolution winds from BLR and WS signatures: one is based on the use of Wavelet Transforms [19, 25–28] and the second on the computation of local gradients [17]. The former methods rely on the ability of wavelets to detect linear structures on SAR images by performing a multiscale analysis. The LG method has been used for a number of applications such as operational SAR wind retrieval [29], wind resource assessment [6], and extreme events monitoring [30, 31], being part of observing and forecasting systems [32] as well. Therefore, LG method has been validated against in situ observations and NWM outputs to obtain wind direction retrievals with an accuracy of 20–30° [18], thereby showing a good performance on wind speed retrieval in offshore areas.

In this paper a modified version of LG, called LG-Mod [33], is proposed. In contrast to the standard LG method, LG-Mod approach is able to extract the dominant local wind direction directly from the set of the available local directions, thus avoiding time-consuming operations on histogram analysis (i.e., histogram binning, weighting, and smoothing), which are commonly required to perform such analysis. In addition, the presented method provides the accuracy related to each wind direction estimate by exploiting basic results from Directional Statistics [34–36].

The paper is structured as follows: the LG-Mod scheme is described in Section 2 and an example of processing is provided by comparing results from a TerraSAR-X image and wind data obtained by the Eta atmospheric model; then, the LG-Mod method is extensively validated against in situ wind data collected by instrumented buoys over coastal areas by using 63 Envisat SAR images. Finally, the main conclusions are drawn in Section 4.

2. LG-Mod Method

The LG-Mod method consists in the following basic steps.

(i) Image Smoothing and Subsampling. According to the LG algorithm [17], SAR image smoothing includes those operations aimed both at mitigating the SAR speckle noise of the input calibrated image and at enhancing the detection of wind-induced patterns (i.e., *wind rows*) on the SAR image. Such smoothing operations should be edge-preserving in order to preserve the directional information of the SAR detected wind structures. The latter is further accomplished by reducing the pixel size to values which are suitable to the best detection of the quasi-periodic, quasi-linear wind-induced features. Typical values range from 100 m to 400 m for the detection of wind rows, thus allowing a multiscale spatial analysis of the SAR signatures.

(ii) Local Gradients (LGs) Computation. An optimized derivative Sobel operator is applied on the SAR amplitudes to estimate the directional features through local gradients determination. This step is performed on pixel basis after removing from the SAR resized image all pixels which are deemed unusable, such as land pixels or those affected by unwanted border effects as a result of the processing performed at the previous step [17].

(iii) Main Directions Extraction. It represents the novel approach of the LG-Mod with respect to the standard LG method. The resized image of local directions is divided into specific size subimages (hereafter also referred to as ROIs), according to the spatial grid on which the wind direction is requested by the user. For each ROI, the dominant direction inside the ROI is directly retrieved by the whole set of the previously estimated directions. Then, the LG-Mod method provides a measure of accuracy for each estimate by developing basic results from Directional Statistics [34, 35]. In particular, as local direction θ and the opposite direction $\theta \pm \pi$ (radians) are equivalent in a circle, the local angles used for estimations should be intrinsically considered as *axial data* instead of *circular data*. The standard way of handling axial data is to convert them to circular data by "doubling the angles," that is, transforming θ to 2θ and so ignoring the ambiguity in direction. Thus, given the set of the observed and usable LG directions $\{\beta_i^{\mathrm{ROI}}\}_{i=1}^{N}$, the mean angle $\langle \beta^{\mathrm{ROI}} \rangle$ and the related accuracy R^{ROI} are, respectively, provided by the following halved phase

$$\left\langle \beta^{\mathrm{ROI}} \right\rangle = \frac{1}{2} \arctan 2 \left(\left\langle \sin\left(2\beta_i^{\mathrm{ROI}}\right) \right\rangle, \left\langle \cos\left(2\beta_i^{\mathrm{ROI}}\right) \right\rangle \right) \ [\mathrm{rad}] \tag{1}$$

and by the amplitude of the so-called *Mean Resultant Vector*, as expressed by

$$R^{\mathrm{ROI}} = \sqrt{\left\langle \cos\left(2\beta_i^{\mathrm{ROI}}\right) \right\rangle^2 + \left\langle \sin\left(2\beta_i^{\mathrm{ROI}}\right) \right\rangle^2}. \tag{2}$$

The mean resultant length R^{ROI} is a nondimensional parameter which represents a measure of the alignment of the directions inside the ROI.

(iv) Reliable ROIs Selection and Estimations. Finally, specifications about the LG-Mod outcomes are fixed directly by the user by adopting a selection criterion to select reliable estimates. Regardless of the statistical distribution of the available directional (axial) data, to each direction estimate, $\langle \beta^{\mathrm{ROI}} \rangle$, an $(1 - \alpha)$ interval of confidence, $\mathrm{ME}_\alpha^{\mathrm{ROI}}$, can be assigned according to the following expression [35, 36]:

$$\mathrm{ME}_\alpha^{\mathrm{ROI}} = \frac{1}{2} \arcsin\left(u_\alpha \sqrt{\frac{\left(1 - \alpha_2^{\mathrm{ROI}}\right)}{2N_{\mathrm{ROI}} \left(R^{\mathrm{ROI}}\right)^2}} \right) \ [\mathrm{rad}], \tag{3}$$

where u_α is the upper $(1/2)\alpha$ quantile of the standard normal distribution and $\alpha_2^{\mathrm{ROI}} = \langle \cos(4(\beta_i^{\mathrm{ROI}} - \langle \beta^{\mathrm{ROI}} \rangle)) \rangle$ represents the second central trigonometric moment of the doubled local directions of the ROI. Expression (3) is valid for ROIs with a large size of samples, N_{ROI}.

Therefore, the LG-Mod method is able to discharge noisy ROIs (and related estimates) by setting a suitable threshold value of acceptance $\mathrm{ME}^{\mathrm{TH}}$ for the estimate $\langle \beta^{\mathrm{ROI}} \rangle$:

$$\mathrm{ROI}_{\mathrm{rel}} = \left\{ \mathrm{ROI} \mid \mathrm{ME}_\alpha^{\mathrm{ROI}} \leq \mathrm{ME}^{\mathrm{TH}} \right\}. \tag{4}$$

Table 1: Comparison results between Eta model and LG-Mod directions for different thresholding selection ($\alpha = 0.05$ and $\mathrm{ME}^{\mathrm{TH}} = 15^\circ, 10^\circ$, and 5°) and for the case of no thresholding.

	RMSE [°]	MBE [°]	Number of wind vectors
No thresholding	26.3	8.2	1616
Thresholding ($\alpha = 0.05$; $\mathrm{ME}^{\mathrm{TH}} = 15^\circ$)	21.1	6.4	1412
Thresholding ($\alpha = 0.05$; $\mathrm{ME}^{\mathrm{TH}} = 10^\circ$)	16.5	3.8	1238
Thresholding ($\alpha = 0.05$; $\mathrm{ME}^{\mathrm{TH}} = 5^\circ$)	7.7	−0.4	578

As an example, the wind field obtained from the X-band TerraSAR-X ScanSAR Multi look Ground range Detected (MGD) image is reported. The SAR image was acquired on February 28, 2010, at 05:44 UTC, with a pixel size equal to 8.5 m, subsequently resampled at 68 m × 68 m. The retrieved wind directions were compared with the ones provided by the Eta numerical weather model [37], which was also used to remove the 180° ambiguity on the wind direction. Eta outputs were provided within a grid of 4 km × 4 km at 06:00 UTC, that is, with a temporal shift of 15 min with respect to the satellite acquisition time.

In Figure 1(a) the LG-Mod estimates of wind directions (red arrows) are shown over the Eta grids; the Eta model predictions are superimposed (yellow arrows). From a visual inspection, it can be clearly seen that both wind direction fields are in good agreement with each other, with the exception of the areas where (1) wind rows are not visible (e.g., the left and the bottom part of the image; the wind shadowed zones near the coastline) and (2) in the middle upper part of the image which is featured by the propagation of an atmospheric gravity wave. After thresholding selection ($\alpha = 0.05$; $\mathrm{ME}^{\mathrm{TH}} = 5^\circ$), the wind field shown in Figure 1(b) was obtained.

The SAR retrieved wind directions were assessed by evaluating their root mean square error (RMSE) and mean bias error (MBE), using Eta model as truth reference. Results of this comparison are reported in Table 1 for different threshold values $\mathrm{ME}^{\mathrm{TH}}$ with confidence level of 95% assigned to the confidence interval of each estimate. The case of no thresholding is also shown in the Table 1 for comparison.

As expected, the tighter the requirements on the assumed accuracy of directional estimates, the lower the estimation error. Accordingly, the number of valid wind estimates progressively reduces. It is worth noting that the accuracy performance of the LG-Mod not only is related to the actual wind conditions but also could depend on SAR system factors, such as the radiometric resolution, which may affect the overall visibility of wind features on the image. This means that a maximum attainable accuracy level has to be expected for a selected SAR sensor. This is the case for ENVISAT SAR imagery for which the highest attainable accuracy was about 15°, as described in the next section.

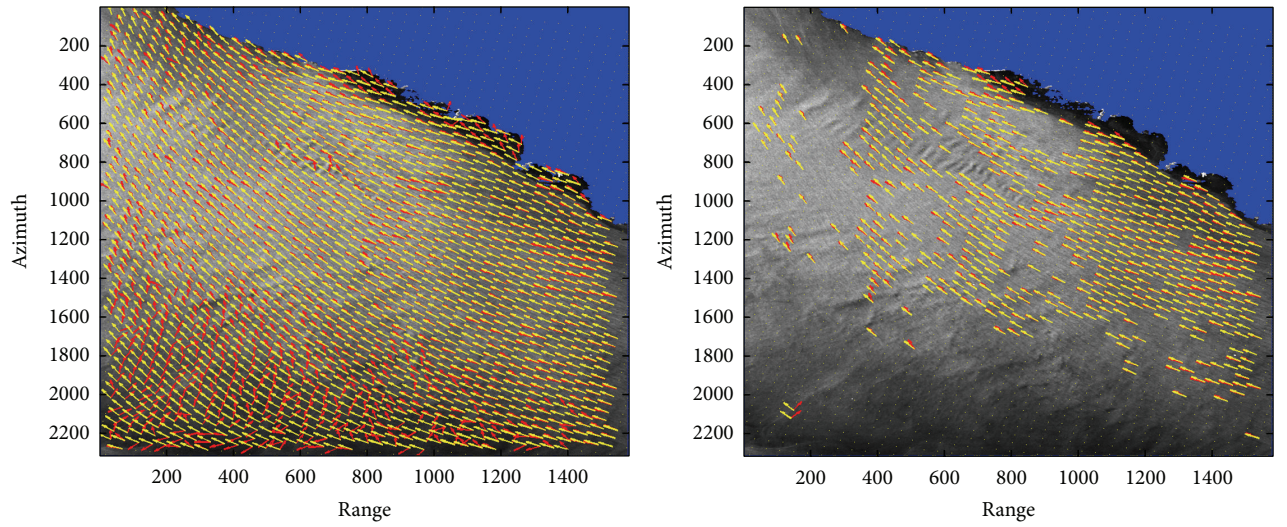

Figure 1: Wind directions estimated over a grid of about 4 km × 4 km by the LG-Mod algorithm (red arrows) and the Eta model (yellow arrows). LG-Mod outcomes are shown before (a) and after (b) discharging unreliable estimations by thresholding selection ($\alpha = 0.05$; $\mathrm{ME}^{\mathrm{TH}} = 5^{\circ}$). The processed full-frame TerraSAR-X ScanSAR MDG image was acquired on February 28, 2010, 05:44:48.110, with VV polarization, descending pass, and off-shore Nice (France), and resized to a pixel size of 68 m × 68 m (background).

Table 2: Information about the buoys deployment and anemometers positioning.

Buoy ID	Geographic coordinates (Lat/Lon) [deg]	Distance from coastline [m]	Sea floor depth [m]	Height of anemometer (above sea level) [m]
62301	52.22 N/4.42 W	≈2600	≈13	3.0
62303	51.60 N/5.10 W	≈3400	≈24	3.0

3. Results

In order to evaluate how the LG-Mod performances in coastal regions, a validation analysis was carried out on a dataset of ENVISAT ASAR images acquired at C-band during the period from 2009 to 2012 in correspondence of two marine coastal areas off-shore Wales (UK). The data have been downloaded from the European Space Agency rolling archives. The two stations were instrumented with buoys belonging to the National Data Buoy Center (NDBC) to hourly collect physical parameters of the marine and atmospheric environment (i.e., wind speed and direction, water and air temperature, air pressure, etc.). In Table 2 relevant information about the buoys deployment and anemometers positioning is reported.

The LG-Mod estimation of the wind directions was carried out on a dataset composed of 63 descending and ascending pass ENVISAT ASAR images, 23 and 40 images in correspondence of 62301 and 62303 buoys, respectively. SAR images were Wide Swath Mode products, with pixel size of 75 m × 75 m. All the SAR products were in the Precision Image (PRI) format and VV polarization. All the available images were radiometrically calibrated with NEST (Next ESA SAR Toolbox) package provided by the ESA (European Space Agency) and preprocessed to get a pixel size of about 150 m × 150 m.

The SAR wind was estimated over squared patch of the SAR image with sizes of 3.6 km, centered on the pixel corresponding to buoy location.

Wind speeds measured by anemometers were collected every hour at the height of 3 m above the sea level (a.s.l.) for both sites. Thus, in order to compare these measurements with the corresponding SAR wind vectors, the instrumental wind speeds were referred to at the height of 10 m a.s.l. [38].

In order to correctly compare each anemometer measurement with the corresponding SAR-based estimation, buoy wind data were linearly interpolated to the SAR acquisition times.

After applying the procedure described in the previous sections, 180° ambiguous wind directions are retrieved for each patch. To resolve the ambiguity in the wind direction, the buoy wind data, interpolated to the time of SAR, were used. For each patch, the retrieved ambiguous direction is compared against the buoys direction, and the one with smaller angular difference is selected. After 180° ambiguity removal, the retrieved wind directions, along with the average SAR Normalized Radar Cross Section (NRCS) value and the mean incidence angle, were computed to estimate the corresponding wind speed using the Geophysical Model Function (GMF) CMOD5.N [39].

Table 3: Statistical results for different subsets.

Dataset	Wind direction RMSE [°]	Wind direction MBE [°]	Wind speed RMSE [m/s]	Wind speed MBE [m/s]	Number of images
A	44.11	−10.32	2.99	−0.77	63
B	19.40	−11.05	2.78	−2.17	6
C ($\alpha = 0.05$; $ME^{TH} = 15^{\circ}$)	26.08	−10.45	2.81	−1.89	10

Table 4: The buoy mean wind speed and air/sea difference temperature.

Dataset	Buoy mean wind speed [m/s]	Buoy mean ($T_{air} - T_{sea}$) [°]
A	10.6 ± 3.5	−1.1 ± 2.1
B	15.5 ± 2.2	−0.7 ± 0.9
C ($\alpha = 0.05$; $ME^{TH} = 15^{\circ}$)	11.4 ± 4.3	−0.9 ± 0.9

The analysis has been conducted considering the whole dataset (A) of the available SAR images, a first subset (B) composed by those images selected after a visual inspection and detection of wind rows around the buoys location and a second subset (C) collecting those "reliable" images automatically selected by the application of the final thresholding step (according to (4), with $\alpha = 0.05$; $ME^{TH} = 15^{\circ}$). In Table 3, statistical results, that is, root mean square error (RMSE) and mean bias error (MBE), derived from the cross-comparison between LG-Mod outcomes and in situ data, are reported, for each defined set of images. Obviously, RMSE and MBE definitions with reference to wind directions take into account that directions must be considered as axial data. From Table 3 it results in high wind direction RMSE if the whole data set is considered. Wind direction RMSE reduces to about 20° when considering SAR images with distinct linear signatures (subset B). These SAR images are characterized by high speed wind regime (>10 m/s, see Table 4) which causes strong local gradients. In the case of automatic selection (described in Section 2), the value of RMSE of about 26° is consistent with the previous selection (subset C). Finally, the good performance of LG-Mod in recognizing wind features when compared to the human expert capability should be pointed out. Indeed, the number of SAR images composing subset C is consistent with relaxing on the user accuracy requirement (i.e., $ME^{TH} = 15^{\circ}$).

4. Conclusions

A novel SAR wind direction retrieval scheme, called LG-Mod, is described. It is based on the directional information carried by the local gradients (LGs) directly computed on quasi-linear, quasi-periodic wind induced structures detected on SAR images. These structures can be related either to atmospheric boundary layer phenomena or streaks generated by the action of the wind on the sea surface. The performance of the method was evaluated using 63 SAR images of coastal sites. The detected linear features were compared against in situ measurements of the wind direction provided by instrumented buoys. Considering the limited number of SAR images used in this study, the results presented should be considered as preliminary. Bearing the latter in mind, the following conclusions can be drawn:

(1) The RMSE value of wind direction estimated on SAR images selected after visual detection of wind rows was comparable with literature reports on off-shore case studies. This result is much better than the best performances obtained using inversion scheme based on wind direction provided by NWM [7].

(2) Adoption of a threshold value on ME^{TH} led to selection of SAR images with meaningful wind induced features (subset C). This result is encouraging as a criterion for automated SAR image selection can be envisaged. It is worth to analyze the composition of SAR images belonging to subset C: 50% of them include wind rows which escaped from visual inspection; 10% are in common with subset B; and the remaining 40% of SAR images include strong linear features not related to the wind field. The latter result is not unexpected as a consequence of the complex phenomena occurring in coastal areas.

(3) It should be expected that a significant number of SAR images belonging to subset B were in common with subset C. Instead, only one SAR image belonging to subset B entered in subset C. It frequently happened that the alignment of detected streaks on SAR images showed an angular dispersion much more prominent than that observed in open sea. This could be explained as the effect of small scale coastal circulation. Although most wind cells were dominated by high directional noise, it was still possible to recognize a dominant direction characterized by strong gradient.

Conflict of Interests

The authors declare that there is no conflict of interests regarding the publication of this paper.

Acknowledgment

The activities described in this paper have been funded by the Italian Flagship Project RITMARE.

References

[1] K. S. Friedman, T. D. Sikora, W. G. Pichel, P. Clemente-Colón, and G. Hufford, "Using spaceborne synthetic aperture radar to improve marine surface analyses," *Weather and Forecasting*, vol. 16, no. 2, pp. 270–276, 2001.

[2] D. B. Chelton, M. H. Freilich, J. M. Sienkiewicz, and J. M. Von Ahn, "On the use of QuikSCAT scatterometer measurements of surface winds for marine weather prediction," *Monthly Weather Review*, vol. 134, no. 8, pp. 2055–2071, 2006.

[3] H. A. Espedal and T. Wahl, "Satellite SAR oil spill detection using wind history information," *International Journal of Remote Sensing*, vol. 20, no. 1, pp. 49–65, 1999.

[4] G. De Carolis, M. Adamo, G. Pasquariello, D. De Padova, and M. Mossa, "Quantitative characterization of marine oil slick by satellite near-infrared imagery and oil drift modelling: the Fun Shai Hai case study," *International Journal of Remote Sensing*, vol. 34, no. 5, pp. 1838–1854, 2013.

[5] C. B. Hasager, M. Badger, A. Peña, X. G. Larsén, and F. Bingöl, "SAR-based wind resource statistics in the Baltic Sea," *Remote Sensing*, vol. 3, no. 1, pp. 117–144, 2011.

[6] M. B. Christiansen, W. Koch, J. Horstmann, C. B. Hasager, and M. Nielsen, "Wind resource assessment from C-band SAR," *Remote Sensing of Environment*, vol. 105, no. 1, pp. 68–81, 2006.

[7] M. Adamo, F. M. Rana, G. De Carolis, and G. Pasquariello, "Assessing the Bayesian inversion technique of C-band synthetic aperture radar data for the retrieval of wind fields in marine coastal areas," *Journal of Applied Remote Sensing*, vol. 8, no. 1, Article ID 083531, 2014.

[8] M. Portabella, A. Stoffelen, and J. A. Johannessen, "Toward an optimal inversion method for synthetic aperture radar wind retrieval," *Journal of Geophysical Research C: Oceans*, vol. 107, no. 8, pp. 1–13, 2002.

[9] T. M. Weckwerth, J. W. Wilson, R. M. Wakimoto, and N. A. Crook, "Horizontal convective rolls: determining the environmental conditions supporting their existence and characteristics," *Monthly Weather Review*, vol. 125, no. 4, pp. 505–526, 1997.

[10] S. Khanna and J. G. Brasseur, "Three-dimensional buoyancy- and shear-induced local structure of the atmospheric boundary layer," *Journal of the Atmospheric Sciences*, vol. 55, no. 5, pp. 710–743, 1998.

[11] T. M. Weckwerth, T. W. Horst, and J. W. Wilson, "An observational study of the evolution of horizontal convective rolls," *Monthly Weather Review*, vol. 127, no. 9, pp. 2160–2179, 1999.

[12] P. Drobinski and R. C. Foster, "On the origin of near-surface streaks in the neutrally-stratified planetary boundary layer," *Boundary-Layer Meteorology*, vol. 108, no. 2, pp. 247–256, 2003.

[13] D. Etling and R. A. Brown, "Roll vortices in the planetary boundary layer: a review," *Boundary-Layer Meteorology*, vol. 65, no. 3, pp. 215–248, 1993.

[14] W. Alpers and B. Brummer, "Atmospheric boundary layer rolls observed by the synthetic aperture radar aboard the ERS-1 satellite," *Journal of Geophysical Research*, vol. 99, no. 6, pp. 12613–12621, 1994.

[15] T. W. Gerling, "Structure of the surface wind field from the Seasat SAR," *Journal of Geophysical Research*, vol. 91, no. 2, pp. 2308–2320, 1986.

[16] H. Dankert, J. Horstmann, and W. Rosenthal, "Ocean wind fields retrieved from radar-image sequences," *Journal of Geophysical Research C: Oceans*, vol. 108, no. 11, pp. 3352–3364, 2003.

[17] W. Koch, "Directional analysis of SAR images aiming at wind direction," *IEEE Transactions on Geoscience and Remote Sensing*, vol. 42, no. 4, pp. 702–710, 2004.

[18] W. Koch and F. Feser, "Relationship between SAR-derived wind vectors and wind at 10-m height represented by a mesoscale model," *Monthly Weather Review*, vol. 134, no. 5, pp. 1505–1517, 2006.

[19] G. Levy, "Boundary layer roll statistics from SAR," *Geophysical Research Letters*, vol. 28, no. 10, pp. 1993–1995, 2001.

[20] F. Fetterer, D. Gineris, and C. C. Wackerman, "Validating a scatterometer wind algorithm for ERS-1 SAR," *IEEE Transactions on Geoscience and Remote Sensing*, vol. 36, no. 2, pp. 479–492, 1998.

[21] S. Lehner, J. Horstmann, W. Koch, and W. Rosenthal, "Mesoscale wind measurements using recalibrated ERS SAR images," *Journal of Geophysical Research C: Oceans*, vol. 103, no. 4, pp. 7847–7856, 1998.

[22] C. C. Wackerman, C. L. Rufenach, R. A. Shuchman, J. A. Johannessen, and K. L. Davidson, "Wind vector retrieval using ERS-1 synthetic aperture radar imagery," *IEEE Transactions on Geoscience and Remote Sensing*, vol. 34, no. 6, pp. 1343–1352, 1996.

[23] C. C. Wackerman, W. G. Pichel, and P. Clemente-Colon, "Automated estimation of wind vectors from SAR," in *Proceedings of the 12th Conference on Interactions of the Sea and Atmosphere*, Long Beach, Calif, USA, February 2003.

[24] H. Lin, Q. Xu, and Q. Zheng, "An overview on SAR measurements of sea surface wind," *Progress in Natural Science*, vol. 18, no. 8, pp. 913–919, 2008.

[25] Y. Du, P. W. Vachon, and J. Wolfe, "Wind direction estimation from SAR images of the ocean using wavelet analysis," *Canadian Journal of Remote Sensing*, vol. 28, no. 3, pp. 498–509, 2002.

[26] N. Fichaux and T. Ranchin, "Combined extraction of high spatial resolution wind speed and wind direction from SAR images: a new approach using wavelet transform," *Canadian Journal of Remote Sensing*, vol. 28, no. 3, pp. 510–516, 2002.

[27] G. C. Leite, D. M. Ushizima, F. N. S. Medeiros, and G. G. de Lima, "Wavelet analysis for wind fields estimation," *Sensors*, vol. 10, no. 6, pp. 5994–6016, 2010.

[28] S. Zecchetto and F. De Biasio, "A wavelet-based technique for sea wind extraction from SAR images," *IEEE Transactions on Geoscience and Remote Sensing*, vol. 46, no. 10, pp. 2983–2989, 2008.

[29] J. Horstmann and W. Koch, "Evaluation of an operational SAR wind field retrieval algorithm for ENVISAT ASAR," in *Proceedings of the IEEE International Geoscience and Remote Sensing Symposium*, pp. 44–47, ACM, Anchorage, Alaska, USA, September 2004.

[30] E. V. Stanev, J. Schulz-Stellenfleth, J. Staneva, S. Grayek, J. Seemann, and W. Petersen, "Coastal observing and forecasting system for the German bight—estimates of hydrophysical states," *Ocean Science*, vol. 7, no. 5, pp. 569–583, 2011.

[31] R. P. Signell, J. Chiggiato, J. Horstmann, J. D. Doyle, J. Pullen, and F. Askari, "High-resolution mapping of Bora winds in the northern Adriatic Sea using synthetic aperture radar," *Journal of Geophysical Research: Oceans*, vol. 115, no. 4, 2010.

[32] J. Horstmann, W. Koch, D. R. Thompson, and H. Graber, "Observation of hurricane winds using synthetic aperture radar," in *Proceedings of the Advances in SAR Oceanography from ENVISAT and ERS Missions (SeaSAR '06)*, ESA SP-613, Frascati, Italy, January 2006.

[33] F. M. Rana, M. Adamo, G. Pasquariello, G. De Carolis, S. Morelli, and F. Bovenga, "A simplified local gradient method for the retrieval of SARderived sea surface wind directions," in *Proceedings of the 10th European Conference on Synthetic Aperture Radar (EUSAR '14)*, Berlin, Germany, June 2014.

[34] K. V. Mardia and P. E. Jupp, *Directional Statistics*, vol. 494, John Wiley & Sons, New York, NY, USA, 1999.

[35] N. I. Fisher, *Statistical Analysis of Circular Data*, Cambridge University Press, Cambridge, UK, 1995.

[36] N. I. Fisher and T. Lewis, "Estimating the common mean direction of several circular or spherical distributions with differing dispersions," *Biometrika*, vol. 70, no. 2, pp. 333–341, 1983.

[37] F. Mesinger, S. C. Chou, J. L. Gomes et al., "An upgraded version of the Eta model," *Meteorology and Atmospheric Physics*, vol. 116, no. 3-4, pp. 63–79, 2012.

[38] H. K. Johnson, "Simple expressions for correcting wind speed data for elevation," *Coastal Engineering*, vol. 36, no. 3, pp. 263–269, 1999.

[39] H. Hersbach, *CMOD5. N: A C-Band Geophysical Model Function for Equivalent Neutral Wind*, European Centre for Medium-Range Weather Forecasts, 2008.